4th International Conference on Molten Slags and Fluxes, 1992, Sendai, ISIJ

# RATE OF DISSOLUTION OF SOLID ALUMINA INTO MOLTEN SLAGS

Hiroyuki Naito*, Masahiro Isomoto**, Makoto Kishimoto***
Kunihiko Nakashima*** and Katsumi Mori***

*Kokura Works, Sumitomo Metal Ind. Ltd., Japan
**Nagasaki Shipyard and Machinery Works, Mitsubishi Heavy Ind. Ltd., Japan
***Department of Materials Science and Engineering, Faculty of Engineering, Kyushu University, Japan

**Synopsis:** The dissolution rate of alumina into molten $CaO-SiO_2-Al_2O_3$(BF-type) and $Na_2O-SiO_2$ (soda silicate) slags were examined by the rotating cylinder method. The dissolution rates increased with increasing revolution speed. The apparent activation energies for mass transport in BF-type and in soda silicate slags were calculated to be 186 and 113kJ/mol, respectively. These results show that the dissolution rate of alumina was concluded to be limited by mass transport in a slag boundary layer.

It was found from EPMA analysis of specimen after experiments that slag components, Ca and Si, penetrated into grain boundary of alumina and a compound, $CaO \cdot 6Al_2O_3$, was produced in the penetration layer for BF-type slags. On the other hand, such a penetration layer and any compounds were not found for soda silicate slags.

**Key words:** sintered alumina cylinder, dissolution rate, molten slag, $CaO-SiO_2-Al_2O_3$, $Na_2O-SiO_2$, slag attack of refractories, slag penetration, $CaO \cdot 6Al_2O_3$.

## 1. Introduction

The dissolution of solid oxides into molten slags is related to furnace life, slagging and the absorption of nonmetallic inclusions by mold fluxes. Therefore, the dissolution behavior of solid oxides into molten slags is an important problem in refining processes.

Alumina is one of refractory materials widely used in pyrometallurgical processes as well as a main deoxidation product in steel-making process. Many investigations on the reaction between alumina and slag have been carried out from the standpoints of the dissolution loss of refractories and the absorption or the dissolution of inclusions[1]-[3]. On the other hand, slags which are different in system and composition from conventional ones have been used in smelting processes. However, the effects of composition of such advanced slags or stirring intensity on the dissolution behavior have not yet been investigated sufficiently.

In the present work, to clarify the dissolution behavior of alumina into molten slags, the dissolution rates of sintered alumina into molten $CaO-SiO_2-Al_2O_3$(BF-type) and $Na_2O-SiO_2$(soda silicate) slags were examined by the rotating cylinder method used in the previous works[4][5]. In addition, the penetration of molten slags into an alumina cylinder and the formation of compounds were examined by EPMA and X-ray diffraction analysis.

## 2. Experimental procedures

### 2-1. Preparation of sintered alumina cylinder

Alumina powder of 99.8% purity, arabian gum and distilled water were thoroughly mixed in the ratio of 90:5:5 by weight. Thirty grams of this mixture was pressed into a cylindrical shape and was sintered at 1823K for 90 min in air. The sintered cylinder was 17 mm in diameter and 32 mm in length, and the bulk density and the apparent porosity were 3.97 $g/cm^3$ and 1 %, respectively.

### 2-2. Preparation of synthetic slags

The mixing ratios of slags used are shown in Table 1. Synthetic slags were prepared by melting mixtures of reagent grade $CaCO_3$, $SiO_2$, $Al_2O_3$ and $Na_2CO_3$ powders in a crucible (graphite for BF-type slags and steel for soda silicate slags) under argon atmosphere, followed by quenching on an iron plate.

Table 1 Chemical composition of slags. (mass%)
(a)BF-type slags (b)Soda silicate slags. (R=molar ratio)

| Slag | CaO | $SiO_2$ | $Al_2O_3$ |
|---|---|---|---|
| A | 45 | 45 | 10 |
| B | 40 | 40 | 20 |
| C | 35 | 35 | 30 |

| Slag | $Na_2O$ | $SiO_2$ | R |
|---|---|---|---|
| D | 68 | 32 | 2 |
| E | 50 | 50 | 1 |
| F | 44 | 56 | 0.75 |
| G | 34 | 66 | 0.50 |

## 2-3. Experimental method

A schematic diagram of the experimental apparatus is shown in Fig. 1. The synthetic slag was melted at the experimental temperature under argon atmosphere. Then the depth of the slag bath was 70 mm. After being preheated, the cylinder was immersed in the slag bath and rotated at a fixed revolution speed. The temperature was measured by a Pt/Pt-13%Rh thermocouple at the mid-depth of the slag bath and was held constant within ±5°C. The cylinder was withdrawn from the slag bath after immersion for predetermined periods.

After the remaining slags on the surface of the cylinder was dissolved by a HCl dilute solution or hot water, the diameters of the cylinder were measured by a micrometer.

The alumina cylinder after experiment was analyzed by EPMA and X-ray diffraction analysis in order to examine the penetration of molten slags and the formation of compounds.

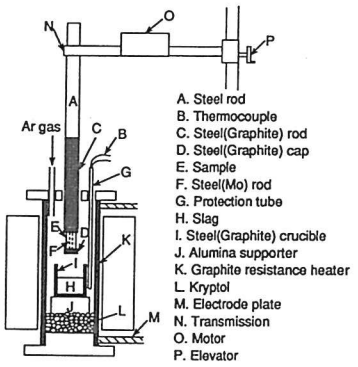


Fig. 1 Experimental apparatus.

## 3. Experimental results

In Fig. 2 and 3, the effect of the revolution speed on the dissolution rate of sintered alumina into BF-type slag A and soda silicate slag E are shown as a function of the decrease in the radius of cylinder against the immersion time. These figures indicate that the radius of cylinder decreases linearly with immersion time and that the slopes of these lines increase with increasing revolution speed. These results indicate that the dissolution process of sintered alumina into both molten slags is controlled by mass transport in slag.

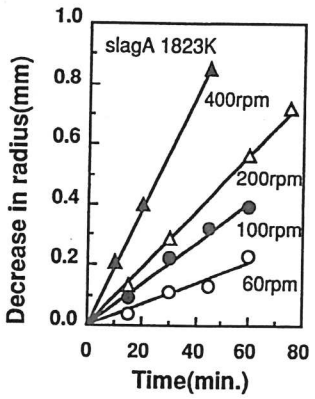


Fig. 2 Effect of revolution speed on the dissolution rate of alumina into slag A.

When mass transfer in a liquid boundary layer is a rate-controlling step, the flux, J, of solute transferred across the interface can be expressed by the following equation;

$$J=k(n_s-n_b) \quad (1)$$

where k is mass transfer coefficient (cm/s), n is mass density of a solute in liquid slag ($g/cm^3$) and subscript s and b indicate the interface and the bulk of liquid, respectively. The relationship between J and the decreasing rate of the radius of solid cylinder (-dr/dt) is given from a mass balance of $Al_2O_3$ at the interface as follows;

$$\rho_{solid} \cdot A \cdot (-dr/dt) = A \cdot J \quad (2)$$

where $\rho_{solid}$ and A are the apparent mass density ($g/cm^3$) of the solid and the interfacial area ($cm^2$) between solid and liquid, respectively. When -dr/dt is expressed as V which is a measure of the dissolution rate of a cylinder, the following equation can be obtained by combining Eqs.(1) and (2);

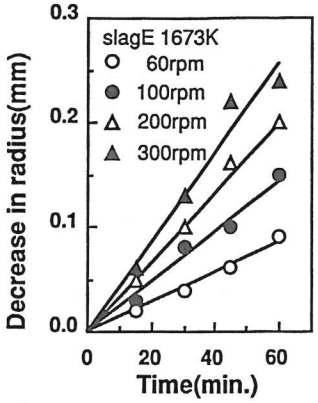


Fig. 3 Effect of revolution speed on the dissolution rate of alumina into slag E.

$$V=k(C_s\rho_s-C_b\rho_b)/100\cdot\rho_{solid}$$

$$=k\cdot\rho_b\cdot\Delta(\%Al_2O_3)/100\cdot\rho_{solid} \quad (3)$$

where C and $\rho$ are mass% of solute and the density of liquid (g/cm$^3$). The experimental conditions and the calculated results are summarized in Table 2. Fig.4 and 5 show the effects of the content of $Al_2O_3$ in BF-type slag ($CaO/SiO_2$=1) and of the molar ratio R ($Na_2O/SiO_2$) of soda slag on the dissolution rate, respectively. The dissolution rate increases with decreasing $Al_2O_3$ content and with increasing molar ratio. Moreover, Kobayashi's results[17] obtained for $Na_2CO_3$-$SiO_2$ slags are plotted for the reference in Fig.5, in which a similar tendency of dissolution rate is seen in the range of $R \leqq 2$ although the porosity of alumina and the slag composition are different. Such a trend may be caused from the nature that $Na_2CO_3$ reacts quickly with $SiO_2$ to decompose into $Na_2O$ under the coexistence of $SiO_2$ [18]. Table 2 also shows that the dissolution rate is considerably influenced by the experimental temperature.

Table 2 Experimental results.

| Slag | Temp. (K) | n (rpm) | Vx10$^6$ (cm·s$^{-1}$) | kx10$^5$ (cm·s$^{-1}$) | $\Delta(\%Al_2O_3)^{(1)}$ (mass%) |
|---|---|---|---|---|---|
| A | 1853 | 200 | 19.0 | 7.12 | 39.5 |
| | 1823 | 60 | 6.29 | 2.54 | 38.0 |
| | | 100 | 11.0 | 4.48 | |
| | | 200 | 15.9 | 6.41 | |
| | | 400 | 30.4 | 12.2 | |
| | 1773 | 200 | 9.83 | 4.42 | 36.0 |
| B | 1823 | 100 | 5.43 | 2.92 | 28.0 |
| | | 200 | 8.78 | 4.84 | |
| | | 300 | 12.1 | 6.51 | |
| | | 400 | 14.2 | 7.61 | |
| C | 1823 | 200 | 3.65 | 2.91 | 18.0 |
| D | 1673 | 100 | 9.72 | 17.6 | 10.0 |
| E | 1673 | 60 | 2.51 | 1.69 | 26.7 |
| | | 100 | 4.22 | 2.84 | |
| | | 200 | 5.50 | 3.70 | |
| | | 300 | 7.36 | 4.95 | |
| | 1573 | 200 | 2.84 | 2.03 | 23.9 |
| | 1473 | 200 | 2.00 | 1.54 | 22.1 |
| | 1373 | 200 | 0.70 | 0.57 | 20.4 |
| F | 1673 | 200 | 1.12 | 0.67 | 29.9 |
| G | 1673 | 200 | 0.44 | 0.35 | 28.8 |

## 4. Discussion

### 4.1 Effect of revolution speed on the dissolution rate of alumina

It was concluded based on the above mentioned results that the diffusion of solute in the molten slag layer around a sintered alumina cylinder was the rate-controlling step. In such a case, the relationship between the dissolution rate, V, and the flow velocity, U, can be expressed as follows;

$$V=B\cdot U^s \quad (4)$$

where B is a constant, s=0.50—0.80 has been reported[4]-[9].

In Fig.6, log V are plotted against log U. Where the periphery velocity of the cylinder (= $\pi$dm/60, d is the mean diameter of cylinder in cm and m is revolutions per minute) is used as U. The linear relationship between log V and log U is found to hold for each slag. Their slopes, i.e. values of s, are calculated to be 0.71 and 0.80 for BF-type slags and 0.66 for soda silicate slag, respectively, and lie within the range of the reported values. This result supports the conclusion that the rate-controlling step of the dissolution of alumina under the present experimental conditions is the diffusion of solute in the slag boundary layer.

In general, some dimensionless correlation is often used to express the relationship between the mass transfer coefficient and the flow condition. When a $J_D$-factor is taken as a dimensionless number, the $J_D$-factor is expressed as a function of Reynolds number, Re(=dU/$\nu$ ) as follows[14],

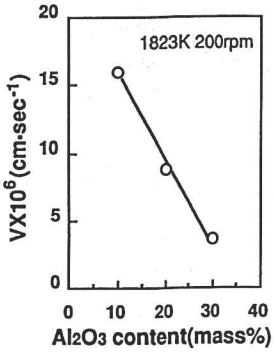


Fig. 4 Relationship between the dissolution rate and $Al_2O_3$ content for BF-type slags.

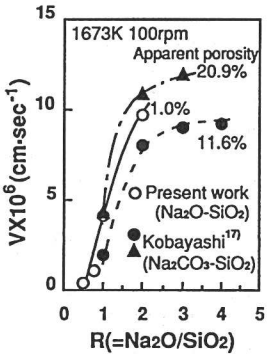


Fig. 5 Relationship between the dissolution rate and molar ratio for soda silicate slags.

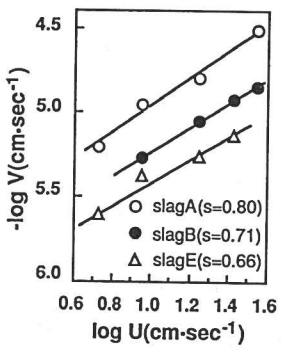


Fig.6 Effect of periphery velocity on the dissolution rate of alumina.

$$J_D=(k/U)(S_c)^a=C(Re)^b \quad (5)$$

where Sc is the Schmidt number (= $\nu$/D), $\nu$ is kinetic viscosity, D is diffusion coefficient and a, b and C are constants. For example, the dissolution rates of benzenic acid in water[5] or of a solid steel in liquid aluminum[7] and the other experimental results have been empirically expressed by Eq.(5) in the wide range of the Reynolds number from $1\times10^2$ to $5\times10^4$. Then the constant, a, was assumed to be 2/3. The value of -0.25 or -0.30 for b was obtained there.

In the calculation of $J_D$-factor, physical properties of slags, especially the diffusivity of solute, are the dominant factors. However there have been only a few investigations on the diffusivity of $Al_2O_3$ in ternary slag systems studied in the present work. Thus the interdiffusion coefficient of $Al_2O_3$ of BF-type slag was estimated from that of a pseudobinary $CaO-Al_2O_3$ slag system[19]. For soda silicate slag, the interdiffusion coefficient of $50\%Na_2O\cdot50\%SiO_2$ slag[10] were used, because this value highly depends on $SiO_2$ content. The physical properties used in the calculation are shown in Table 3. The relationships between $J_D$-factor and Reynolds number for each slag composition are given as follows;

$$J_D=0.060\cdot Re^{-0.21} \quad \text{(slag A)} \quad (6)$$

$$J_D=0.074\cdot Re^{-0.30} \quad \text{(slag B)} \quad (7)$$

$$J_D=0.048\cdot Re^{-0.37} \quad \text{(slag E)} \quad (8)$$

These relationships are illustrated together with the previous investigations in Fig.7. The plots of BF-type slag A and B tend to lie on the extension line of the line 6 for the high temperature experiment. The experiments have been carried out under the same conditions expect for the slag compositions, nevertheless the exponents of Reynolds number and the absolute values of $J_D$-factor are different among these equations. The insufficiency of available date on physical properties and the narrow range of the Reynolds number measured may be considered to be some reason for such differences as mentioned above. Furthermore, the change in the dissolution behavior by slag penetration observed by EPMA analysis as will be seen later may be considered as another reason. The mean value of the interdiffusion coefficients in the bulk and the $Al_2O_3$-saturated slags were used in this calculation. However, the lines shown by Eqs.(6) and (7) shift upward, if the interdiffusion coefficients in $Al_2O_3$-saturated slag is applied. Therefore, the way of the estimation of physical properties is also one of important factors in the calculation of $J_D$-factor.

Table 3 Physical properties of slags.

| Slag | Temp. (K) | $D\times10^6$ ($cm\cdot s^{-1}$) | $\rho_b$ ($g\cdot cm^{-3}$) | $\eta$ (Pa·s) |
|---|---|---|---|---|
| A | 1823 | 1.83[10] | 2.51[12] | 0.33[13] |
| B | | 1.71[10] | 2.57[12] | 0.62[13] |
| C | | | *2.76[13] | *1.10[13] |
| D | 1673 | | 2.20[10] | |
| E | | 1.65[10] | 2.20[10] | *0.30[13] |
| | | 0.41[14] | | |
| F | | | 2.20[10] | *1.30[10] |
| G | | 0.75[10] | 2.20[10] | 2.69[10] |

* estimated values

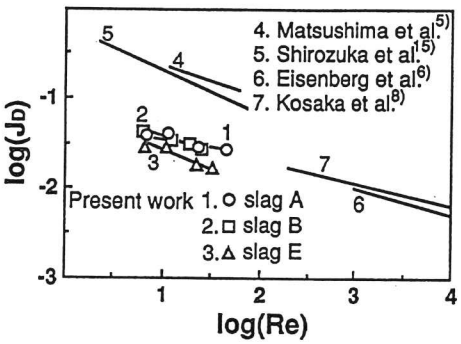


Fig. 7 Relationship between $J_D$-factor and Reynolds number.

There have been no available data on the diffusivity of $Al_2O_3$ in soda silicate slags. So a value of $5\times10^{-7}cm^2/s$ for this property is calculated by assuming that the results of soda silicate slag E can be similarly expressed by equation (7). This value is close to the interdiffusion coefficient of $Na_2O-SiO_2$ system reported by Schwerdtfeger[13].

## 4.2 Temperature dependence of dissolution rate

Figure 8 shows the effect of temperature on the mass transfer coefficient. The linear relationship holds for both slags, and the apparent activation energies for mass transport are calculated to be 186 kJ/mol for slag A and 113 kJ/mol for slag E from the slop of respective line. Rewriting Eq.(5) for k gives the following equation;

$$k=C(U^2d)^b\cdot\eta^{-(a+b)}\cdot\rho_b{}^{(a+b)}\cdot D^a \quad (9)$$

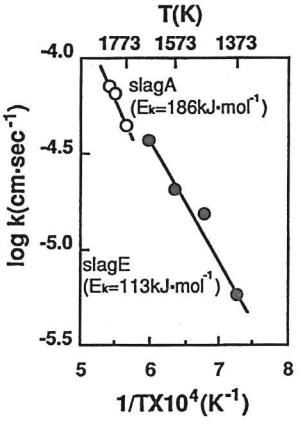


Fig. 8 Effect of temperature on mass transfer coefficient.

Since $\eta$ and D follow the Arrhenius type temperature dependence, the activation energy $E_k$ for mass transport can be expressed by the activation energies $E\eta$ for the viscosity and $E_D$ for the diffusion as follows[15];

$$E_k=(a+b)E\eta+aE_D \qquad (10)$$

Here, the temperature dependence of slag density is neglected. The observed value of apparent activation energies, $E_k^{obs}$ and the calculated activation energies, $E_k^{cal}$ from Eq. (10) are shown together in Table 4. The fact that the observed and the calculated energies approximately agree supports that the dissolution process of solid alumina into molten slag under the present experimental conditions is controlled by mass transport of solute in slags.

Table 4 Apparent activation energies for mass transport in molten slags.

| Slag | $E_k^{obs}$ (kJ·mol$^{-1}$) | $E_k^{cal}$ (kJ·mol$^{-1}$) | $E_D$ (kJ·mol$^{-1}$) | $E\eta$ (kJ·mol$^{-1}$) |
|---|---|---|---|---|
| A | 186 | 195～281 | 240[19]～356[12] | 93[13] |
| E | 113 | 64～131 | 42[18]～142[13] | 121[13] |

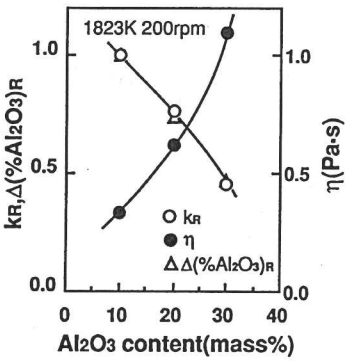


Fig. 9 Variation in physical properties with $Al_2O_3$ content for BF-type slags.

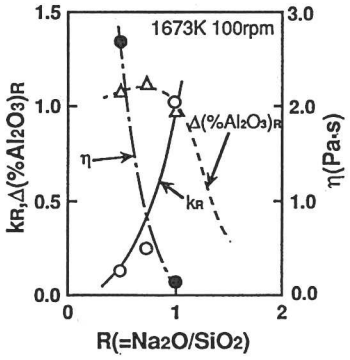


Fig. 10 Variation in physical properties with molar ratios for soda silicate slags.

## 4.3 Dependence of dissolution rate on slag composition

Figure 9 shows the dependences of the viscosity of slag, the mass transfer coefficient, $k_R$, and $\Delta(\%Al_2O_3)_R$ on $Al_2O_3$ content of BF-type slags with $CaO/SiO_2=1$. Where the values of both $k_R$ and $\Delta(\%Al_2O_3)_R$ are expressed as relative values to those for slag A. It is found from this figure that $\Delta(\%Al_2O_3)_R$ as a driving force for mass transport and $k_R$ decrease with increasing $Al_2O_3$ content and the curves for both factors have a nearly equal slope. Consequently, the decrease in dissolution rate with increasing $Al_2O_3$ content as seen in Fig. 4 can be attributed to the decrease in $k_R$ and $\Delta(\%Al_2O_3)_R$, and also these two factors are regarded to have an equivalent influence on the decrease in the dissolution rate.

Figure 10 shows the dependences of the viscosity, and the relative values of mass transfer coefficient $k_R$ and $\Delta(\%Al_2O_3)_R$ to those for slag E(R=1) on molar ratio of soda silicate slag. It is found from Fig. 10 that in the range of $R<2$, $\Delta(\%Al_2O_3)_R$ decreases, but the value of $k_R$ remarkably increases with increasing molar ratio. Therefore, such a increase in $k_R$ may be resulted from the decrease in viscosity of slag.

It is concluded from the facts mentioned above that the increase of the dissolution rate shown in Fig. 5 is caused mainly by increasing mass transfer coefficient.

## 4.4 Dissolution mechanism

Figure 11 shows SEM micrographs and X-ray images in the vicinity of the alumina-slag interface of the cylinder after immersed into slag A at 200rpm and at 1823K for 60 min.

The existence of the slag penetration layer (about 0.5mm in thickness) is confirmed, and the thickness of this penetration layer tends to in-

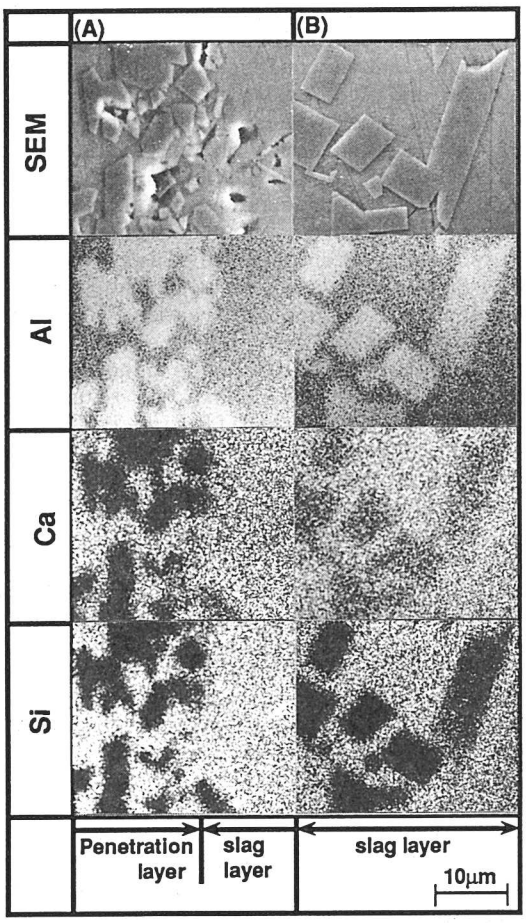


Fig.11 SEM micrographs and X-ray images of alumina-slag interface.

crease with increasing immersion time. Slag components, Ca and Si, are detected around alumina particles in the slag penetration layer as shown in Fig. 11-(A). In the slag layer, coarsened alumina particles are isolated and a slag component, Ca, is detected from these particles as seen in Fig. 11-(B). The existence of such isolated particles implies the possibility that the mechanical separation of some alumina particles occurs simultaneously with the dissolution reaction into slag, as well.

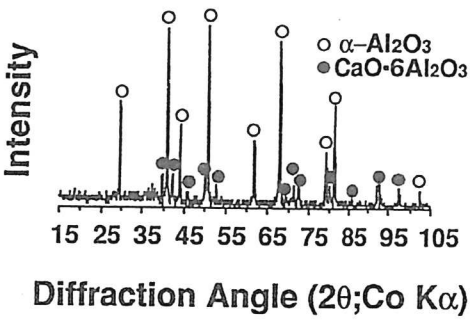


Fig. 12 X-ray diffraction patterns.

Figure 12 shows the X-ray diffraction patterns of the sample taken from the penetration layer shown in Fig. 11. The existence of $CaO \cdot 6Al_2O_3$ besides $\alpha$-$Al_2O_3$ is confirmed. This result suggests that alumina reacts with CaO to form $CaO \cdot 6Al_2O_3$ in BF-type slags A and B. On the other hand, such a slag penetrated layer as observed for BF-type slags was not found for soda silicate slags. And also the X-ray diffraction patterns show the existence of only $\alpha$-$Al_2O_3$.

These results of EPMA analysis, X-ray diffraction and micrographs indicate that the dissolution reaction of solid alumina into BF-type slags proceeds both in the penetration layer of slags and at the surface of alumina cylinder, while that into soda silicate slags proceeds only at the surface of alumina cylinder.

## 5. Conclusions

The effects of revolution speed, temperature and slag composition on the dissolution rate of the sintered alumina into molten $CaO$-$SiO_2$-$Al_2O_3$ and $Na_2O$-$SiO_2$ slags were examined by the rotating cylinder method. At the same time, the penetration of molten slags into alumina and the formation of the compounds were examined by EPMA and X-ray diffraction analysis. The results are summarized as follows;

(1) The dissolution rate of alumina into molten both slag systems increased with increasing revolution speed. Moreover, this result can be expressed by the dimensionless correlation using the $J_D$-factor.

(2) The apparent activation energies for mass transport in BF-type slag and soda silicate slag were calculated to be 186 and 113kJ/mol, respectively.

(3) The penetration of slag components, Ca and Si, into alumina was observed and $CaO \cdot 6Al_2O_3$ compound were formed in the penetration layer for BF-type slags. On the other hand, neither such a penetration layer nor a compound were observed or soda silicate slags.

(4) The rate controlling-step on the dissolution process of alumina into molten both slags systems was found to be the diffusion rate of solute in the slag boundary layer.

## References

1) A.R.Cooper,Jr and W.D.Kingery: J. Am. Ceramic Soc., 47(1964),37.
2) S.Nakato, T.Emi and A.Ejima: Tetsu-to-Hagane, (1974),A15.
3) Y.Araki, Y.Sugitani and S.Ishimura: Tetsu-to-Hagane, (1972),S370.
4) M.Umakoshi, K.Mori and Y.Kawai: Trans. I. S. I. Japan, 67(1981),1762.
5) M.Umakoshi, S.Yadoomaru, K.Mori and Y.Kawai: Trans. I. S. I. Japan, 17(1977),442.
6) M.Eisenberg, C.W.Tobias and C.R.Wilke: Chem. Eng. Prog. Symp. Ser. No16, 51(1955),1.
7) H.Kobayashi and T.Oyama: Yogyo-kyoukai-shi, 82(1974),546.
8) I.Kosaka and S.Minowa: Tetsu-to-Hagane, 52(1966),1748.
9) J.Henderson, L.Yang and G.Derge: Trans. Met. Soc. AIME, 221(1961),56.
10) I.Kosaka, Y,Shiraishi and K.Saitou: Bull. Res. Inst. Min. Press. Metall. Tohoku University, 24(1968),13.
11) Phase Diagrams for ceramists: (1964),181, The Amer. Ceramic Soc. Inc.
12) Youtetsu-Yousai-no-Busseichibinran: (1968), I. S. I. Japan.
13) Handbook of Physico-chemical Properties at High Temperature: ed Y.Kawai and S.Shiraishi, (1988), I. S. I. Japan.
14) K.Schwerdtfeger: J. Phys. Chem., 70(1966),2131.
15) T.Shirozuka, A.Hirata and A.Murakami: Idousokudoron, (1966),168, Oomu-sha .
16) K.Hirota: Hannousokudo, (1957),148, Kyouritsu-syuppan.
17) H.Kobayashi: Tetsu-to-Hagane, 69(1983),1924.
18) Y.Takebayashi, S.Shinozaki, K.Mori and K.Kawai: Tetsu-to-Hagane, 76(1990), 1480.
19) H.Sugawara, K.Nagata and K.S.Goto: Metall.Trans.B, 8B, 12(1977),606.